Short Communication

Facile Synthesis of SnS-Graphene Nanocomposites with High Lithium Storage Capacity

Junsheng Zhu, Dianlong Wang[*]*, Lin Wang, Wanlong You, Qiuming Wang*

School of Chemical Engineering and Technology, Harbin Institute of Technology, Heilongjiang 150001, PR China
[*]E-mail: wangdianlonghit@163.com

SnS-graphene nanocomposites were synthesized through homogeneous precipitation method. The composite material as prepared was characterized using X-ray diffraction, Raman spectroscopy, transmission electron microscopy and elemental analysis. The results indicate that SnS nanoparticles possess a good dispersion on the surface of graphene. The electrochemical performance of SnS-graphene nanocomposites was characterized by galvanostatic charge-discharge tests. The nanocomposites retained a reversible capacity of 679 mAh g^{-1} after 30 cycles. Moreover, the composite material exhibited higher lithium storage capacity and better cycling performance compared to bare SnS and graphene. The results suggest that the combination of SnS and graphene leads to synergistic performance, which enhances electrochemical performance of the overall system.

1. INTRODUCTION

The increasing demands for batteries with higher energy density and better cycle performance have stimulated intense research on lithium-ion batteries (LIBs). Among various anode materials, tin-based composites have attracted intensive attention due to their high capacity, good safety and low cost [1, 2]. In a SnS-based LIBs electrode, Sn alloys with Li forming LixSn (0≤x≤4.4) during lithium alloying process, and gives rise to large volume expansion, which results in the pulverization of the electrode and rapid capacity decrease over extended charge-discharge cycling [3]. To circumvent these problems, a variety of appealing strategies have been applied to improve the lithium storage performance of SnS, such as amorphous carbon-coated SnS [4], net-like SnS/C composite thin-film [5], two-dimensional SnS nanosheets [6].

Recently, graphene have become one of the most promising matrices for metal oxides and metal sulfurs due to their large area, excellent electronic conductivity and open porous structure [7, 8]. Graphene-based composite materials have shown improved electrical conductivity, thermal property, mechanical strength and electrochemical performance [9-11]. Up to now, a number of composite materials consisting of graphene and metal sulfides, such as ZnS [12], SnS2 [13], CdS [14] have been prepared. However, few literatures have reported on SnS-graphene. To expand the extent of graphene-based composites as electrode materials, herein, a facile synthetic approach has been designed to fabricate SnS-graphene nanocomposites. By this means, graphene provide a large contact surface for SnS particles and accommodate the volume change of SnS. Moreover, SnS particles separate graphene and prevent their restacking. The combination of graphene and SnS leads to synergistic performance, which inherits the overall system with enhanced electrochemical performance.

2. EXPERIMENTAL SECTION

2.1 Preparation of sample

Graphene nanosheets (GNS) were synthesized by chemical exfoliation of natural graphite powder by a modified Hummers method [15].

SnS-graphene nanocomposites (SnS-GNS) were prepared by loading SnS on GNS, as described below. 45 mg of GNS, 30 mL of 0.05 mol L^{-1} $SnCl_2$ and 30 mL of 0.05 mol L^{-1} C_2H_5NS were added to a three-neck flask with the capacity of 100 mL. After being mixed fully, the flask was dipped into a hot water bath. The reaction was controlled at 65 ℃ for 3 h. The black deposits were filtered, washed with distilled water and ethanol, and then dried at 60 ℃ under vacuum. For comparison, bare SnS were synthesized via a similar procedure in the absence of GNS precursor.

2.2 Materials Characterization

The microstructures and morphologies of the materials were analyzed by Powder X-ray diffraction (XRD, Rigaku D/MAX-RB), Raman spectroscopy (Jobin Yvon HR800 confocal Raman system with 632.81nm diode laser excitation) and transmission electron microscopy (TEM, JEM-2100F microscope with an accelerating voltage at 200kV), respectively. The content of GNS in SnS-GNS was analyzed by Vario EL cube (Elementar).

2.3 Electrochemical measurements

Electrochemical measurements were carried out using two-electrode cells. The working electrode was prepared by mixing 80 wt.% SnS-GNS, 10 wt.% acetylene black and 10 wt.% polyvinylidene fluorides dissolved in N-methyl-2-pyrrolidone. The resultant slurry was pasted on Cu foil and dried under vacuum. For comparition, SnS electrode and GNS electrode were prepared by the same method. In an argon-filled glove box, the button cells were assembled with a lithium foil as the

counter electrode, Celgard 2300 as the separator, 1 mol L^{-1} $LiPF_6$ in a mixture solvent of ethylene carbonate (EC) and dimethyl carbonate (DMC) (EC:DMC=1:1, by v/v ratio) as the electrolyte. The galvanostatic charge-discharge tests were conducted on Neware Battery Testing System in the voltage range of 0.01 to 3.0 V. Electrochemical impedance spectroscopy measurements were carried out using electrochemical workstation (PARSTAT 2273) over a frequency range from 100000 to 0.01 Hz.

3. RESULTS AND DISCUSSIONS

The XRD patterns of the as-prepared materials are presented in Fig 1a. The diffraction peaks of bare SnS and SnS-GNS agree well with the orthorhombic phase of SnS (JCPDS card No. 39-354), showing good phase purity. In addition, the diffraction peak of graphene at around 21.5° disappear in the SnS-GNS pattern, which indicates that GNS are separated by SnS particles and the amorphous nature of GNS is enhanced by SnS. Moreover, the peaks of SnS-GNS are broad, which indicates that SnS particles are nanosized. The formation of SnS-GNS was further investigated by Raman spectroscopy (Fig. 1b). The broad peaks at 1362 cm^{-1} (D band, κ-point phonons of A_{1g} symmetry) and 1588 cm^{-1} (G band, E_{2g} phonon of C sp^2 atoms) confirm the presence of GNS in the nanocomposites [10].
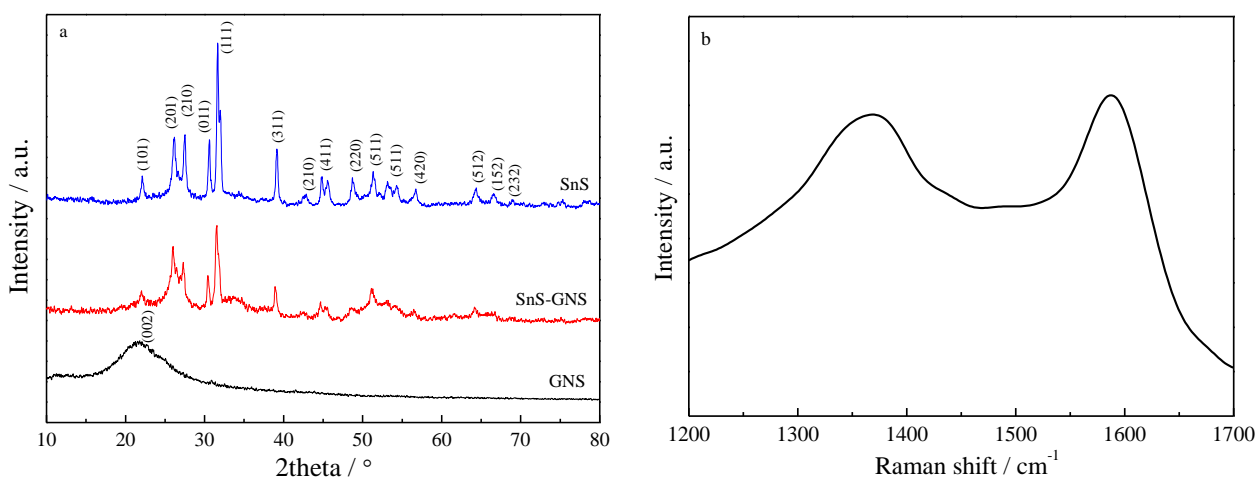
Figure 1. a) XRD patterns of GNS, SnS and SnS-GNS b) Raman spectrum of SnS-GNS

The crystalline structure of SnS-GNS was analyzed by TEM and HRTEM. Fig. 2a shows a low magnification TEM image of SnS-GNS. Worm-like SnS nanoparticles, around 7 nm in diameter, are dispersed uniformly on GNS. HRTEM was employed to further characterize the structure of the nanocomposites. The HRTEM image of the sample with uniform SnS coating (Fig. 2b) displays that the lattice spacing is about 0.28 nm, which agrees with the (111) spacing of SnS. From the HRTEM image of the interface between GNS and SnS, it can be observed clearly that SnS nanoparticles are well wrapped by GNS, which facilitates the homogeneous dispersion of SnS and prevents the

nanoparticles from agglomeration. The mass percentage of GNS in the nanocomposites was analyzed by burning SnS-GNS to form carbon dioxide. The result reveals that SnS-GNS used for electrochemical tests consist of 15 wt.% GNS and 85 wt.% SnS.
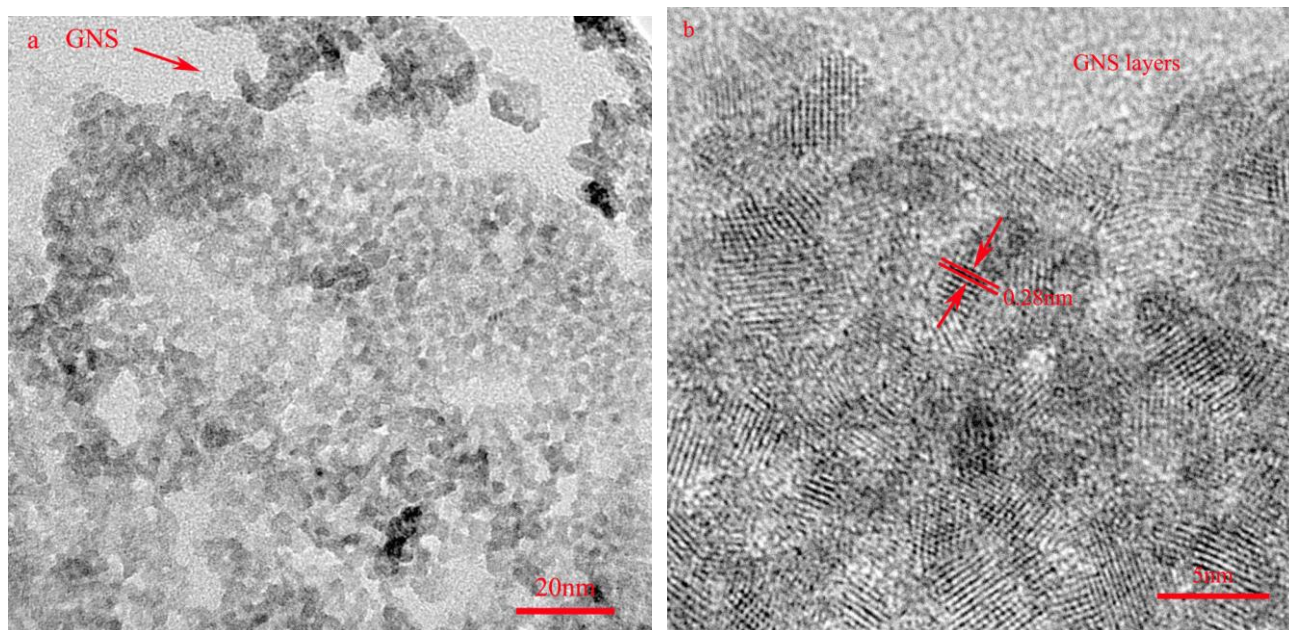

Figure 2. TEM and HRTEM images of SnS-GNS

The lithium storage property of SnS-GNS was investigated by galvanostatic charge/discharge cycling at a current density of 100 mA g^{-1} in the voltage range of 0.01 to 3.0 V. For comparison, bare SnS and GNS were also tested under the same conditions. Fig. 3a,b display the 1st, 2nd, 3rd, and 30th charge/discharge curves of SnS and SnS-GNS anodes, respectively. The first irreversible discharge plateau of SnS-GNS electrode emerges at about 1.25 V, which can be ascribed to the irreversible reduction of SnS to Sn, similar to the characteristics of SnS electrode. Fig. 3c shows the cyclic performances of SnS-GNS, GNS and SnS. The first discharge and charge capacities of SnS-GNS are 1363 and 1060 mAh g^{-1}, respectively. The irreversible capacity may be caused by the reduction of SnS to Sn and the formation of a solid electrolyte interphase [4]. However, in the subsequent charge/discharge cycles, Li-ions are reversibly inserted into Sn as Li$_x$Sn alloys. From the second cycle, the SnS-GNS anode shows highly reversible behavior. The anode exhibits a reversible capacity of 1028 mAh g^{-1}. Moreover, the cycling performancies is enhanced. After 30 cycles, the discharge capacity still remains 679 mAh g^{-1}, which is about 66% retention of the reversible capacity. Compared to the nanocomposites electrode, bare GNS and SnS anodes rapidly lose their capacity over extended charge-discharge cycling. In order to clarify the influence of hybridization on lithium storage performance of SnS-GNS, the theoretical capacity of SnS-GNS is estimated by calculating the capacity of physical mixture of SnS and GNS. According to the theoretical capacity of SnS (782 mAh g^{-1}) and GNS (744 mAh g^{-1}), the theoretical capacity of SnS-GNS is calculated to be 776.3 mAh g^{-1}. Despite the considerable drop, the capacity of the nanocomposites still remains 87.5% of the theoretical value

after 30 cycles. As mentioned above, the enhanced lithium storage property of SnS-GNS can be ascribed to the synergetic effect of SnS and GNS. First, SnS nanoparticles are uniformly distributed on GNS, which prevents the restacking of GNS and facilitates the penetration of electrolyte. During cycling, nanoscale Sn derived from the reduction of SnS nanoparticles could hinder the growth of Li-Sn alloy and aggregation of Sn. Second, the flexible GNS could provide a large contact surface for SnS, which contributes to facile electron transport and prevents the volume change of SnS during alloying-dealloying process.

EIS measurements were carried out to further verify the reason for the improved ithium storage performance of SnS-GNS electrode.
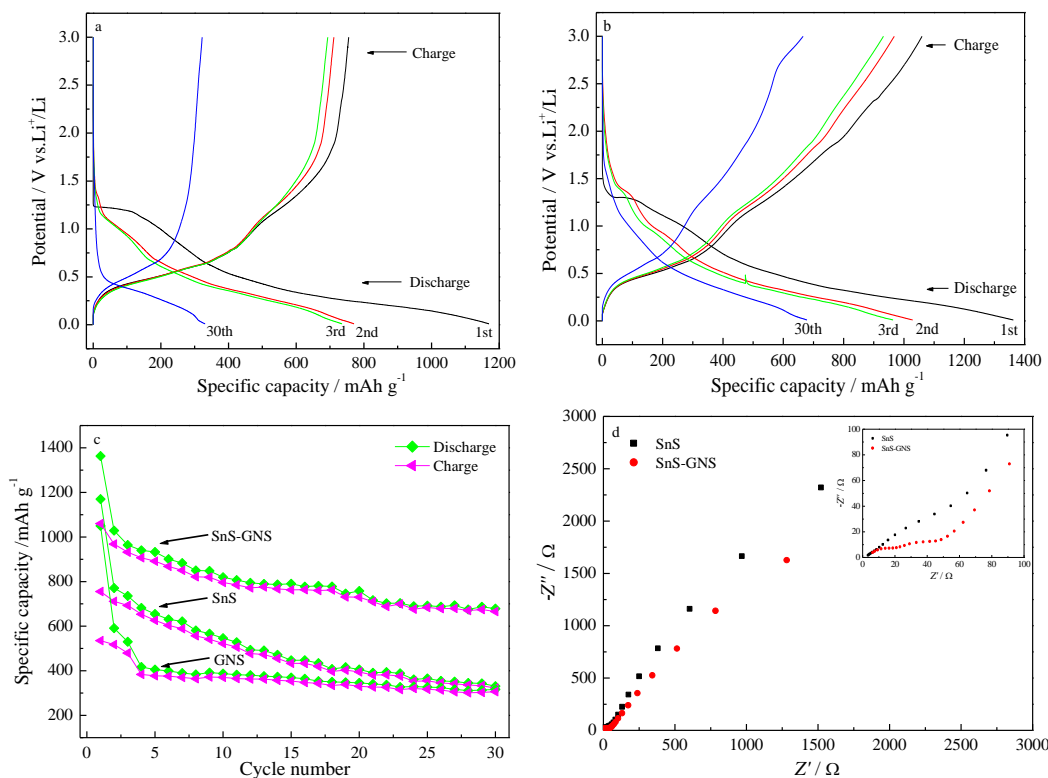
Figure 3. The electrochemical performance of SnS, GNS and SnS-GNS: a) galvanostatic charge/discharge profiles of SnS b) galvanostatic charge/discharge profiles of SnS-GNS c) comparision of the cycle performance of SnS, GNS and SnS-GNS d) the Nyquist plots of the SnS and SnS-GNS

Fig. 3d shows Nyquist plots of bare SnS and SnS-GNS electrodes. The high-frequency semicircle is attributed to SEI film resistance while the spectra in medium frequency is related to charge transfer resistance. From Fig. 3d, the diameter of the semicircle for bare SnS electrode is much bigger than that of SnS-GNS electrode, which indicates that the nanocomposites possess lower charge-transfer resistance. The result shows that the combination of GNS and SnS could improve the electrical conductivity of the overall electrode and enhance the electrochemical activity of SnS. In the nanocomposites, GNS act as conductive matrices while SnS nanoparticles are directly grown on them,

which offers short diffusion length and large quantity of active sites for Li-ions insertion during charge-discharge process. On the other hand, the uniform interaction of GNS and SnS nanoparticles affords a good dispersion of SnS grown on GNS to prevent aggregation of SnS and the restacking of GNS, which enhances cycle stability of the nanocpmposites.

4. CONCLUSION

In this study, SnS nanoparticles anchored onto GNS were prepared by a facile precipitation method. The nanocomposites exhibited enhanced lithium storage capacity. The SnS-GNS electrode showed an initial discharge/charge capacity of 1363/1060 mAh g^{-1}. The discharge capacity still remained 679 mAh g^{-1} after 30 cycles. The enhanced electrochemical performance can be attributed to the synergetic effect of GNS and SnS. Given the easy synthesis and excellent lithium storage property, the method can be extended as a general approach to the preparation of other metal sulfides-graphene nanocomposites.

References

1. Y. Idota, T. Kubota, A. Matsufuji, Y. Maekawa, T. Miyasaka, *Science*, 276(1997)1395.
2. Y. Li, H.Q. Xie, J.P. Tu, *Mater. Lett*., 63(2009)1785.
3. X.L. Gou, J. Chen, P.W. Shen, *Mater. Chem. Phys*., 93(2005)557
4. Y. Li, J.P. Tu, X.H. Huang, H.M. Wu, Y.F. Yuan, *Electrochim. Acta*, 52(2006)1383.
5. Y. Li, J.P. Tu, X.H. Huang, H.M. Wu, Y.F. Yuan, *Electrochem. Commun*., 9(2007)49.
6. J.G. Kang, J.G. Park, D.W. Kim, *Electrochem. Commun*., 12(2010)307.
7. K.S. Novoselov, A.K. Geim, S.V. Morozov, D. Jiang, Y. Zhang, S.V. Dubonos, I.V. Grigorieva, A.A. Firsov, *Science*, 306(2004)666.
8. C.Z. Yuan, L.R. Hou, L. Yang, C.G. Fan, D.K. Li, J.M. Li, L.F. Shen, F. Zhang, X.G. Zhang, *Mater. Lett*., 65(2011)374.
9. Z. Du, X. Yin, M. Zhang, Q. Hao, Y. Wang, T. Wang, *Mater. Lett*., 64(2010)2076.
10. B. Zhao, G.H. Zhang, J.S. Song, Y. Jiang, H. Zhuang, P. Liu, T. Fang, *Electrochim. Acta*, 56(2011)7340.
11. J. Liang, W. Wei, D. Zhong, Q. Yang, L. Li, L. Guo, *ACS Appl. Mater. Interfaces*, 4(2012)454.
12. Y.F. Li, Y.Z. Liu, W.Z. Shen, Y.G. Yang, Y.F. Wen, M.Z. Wang, *Mater. Lett*., 65(2011)2518.
13. K. Chang, Z. Wang, G.C. Huang, H. Li, W.X. Chen, J.Y. Lee, *J. Power Sources*, 201(2012)259.
14. P. Wang, T.F. Jiang, C.Z. Zhu, Y.M. Zhai, D.J. Wang, S.J. Dong, *Nano. Res*., 3(2010)794.
15. Z.S. Wu, W.C. Ren, L.B. Gao, B.L. Liu, C.B. Jiang, H.M. Cheng, *Carbon*, 47(2009)493.